SUPPLEMENTARY INFORMATION

Direct observation of disulfide isomerization in a single protein

Jorge Alegre-Cebollada,[1] Pallav Kosuri,[2] Jaime Andrés Rivas-Pardo,[1,3] and Julio M. Fernández[1]

[1]Department of Biological Sciences, [2]Department of Biochemistry and Molecular Biophysics, Columbia University, New York, 1212 Amsterdam Avenue, 10027 NY, USA. [3]Departamento de Biología, Facultad de Ciencias, Universidad de Chile, Casilla 653, Santiago, Chile.

This section includes:

- Table of contents.
- Supplementary Text.
- 9 Supplementary Figures with legends.
- 2 Supplementary Tables with legends.
- Supplementary References.

TABLE OF CONTENTS

.

SUPPLEMENTARY TEXT

Predicted extensions after cleavage of disulfide bonds.

The magnitude of the extension after the reduction of a disulfide bond under force can be calculated from the number of amino acids that are released in the reaction and the number of disulfides subject to force in the initial and final states. We considered that the contour length per amino acid is 0.4 nm[1]. A contour length of 1.7 nm per disulfide has been proposed before[1]. However, that value was obtained from indirect measurements. The results in Figure 2 in the main text strongly suggest that a value of 0.8 nm is more accurate for the contour length of a cystine residue, because this is the difference in extension between reactions that free the same number of amino acids and only differ in the presence or not of a force-bearing disulfide in the final state (Figure 2).

To account for the fact that our experiments are carried out at a finite force, we used the worm-like chain model of polymer elasticity to calculate the actual extension at a given force (x) from the corresponding contour lengths (L)[2]:

$$\frac{F \cdot p}{K_B \cdot T} = 0.25 \cdot (1 - x/L)^{-2} - 0.25 + x/L \quad \text{(Equation S1)}$$

In Equation S1, F is the force, p is the persistence length of the polypeptide chain, K_B is the Boltzmann constant, and T is the absolute temperature. In our calculations, we considered $K_B \cdot T$ = 4.1 pN·nm and p = 0.3 nm[3,4]. Using Equation S1 at our experimental force (250 pN), x/L is ~0.88. Therefore, the predicted extension after the reduction of a disulfide bond was calculated according to Equation S2:

$$\Delta x_r \text{ (nm, at 250 pN)} = 0.88 \cdot [0.4 \cdot N_{aa} - 0.8 \cdot N_{SS}] \qquad \text{(Equation S2)}$$

In Equation S2, N_{aa} is the number of amino acids released after cleavage of the disulfide and N_{SS} is the difference between the number of force-bearing disulfides before and after the reaction. For instance, in the reduction of the single disulfide in $I27^{32\text{-}75}$, N_{aa} = 43 and N_{SS} = 1, for an expected extension of 14.4 nm. In the intramolecular isomerization reactions, an equal number of force-bearing disulfides are present in the initial and final states, therefore N_{SS} = 0. For instance, in the intramolecular attack by Cys32 on Cys24 to cleave disulfide 24-55, 23 amino acids are released, which translates into an 8.1-nm predicted extension.

The increment in contour length after the mechanical unfolding of $I27^{2S\text{-}S}$ assures that no disulfides other than 24-55 and 32-75 are populated significantly in $(I27^{2S\text{-}S})_4$.

When present in proteins, intramolecular covalent bonds such as disulfides limit the mechanical extension of polypeptide chains at forces below several nanonewtons[1,5,6]. Thus, the disulfides in $I27^{2S\text{-}S}$ must determine the magnitude of the extension after mechanical unfolding of a domain. As for any other polypeptide, after the forced unfolding of $I27^{2S\text{-}S}$, force is transmitted through the shortest way possible. For $I27^{2S\text{-}S}$, this results in the extension of the polypeptide chain between amino acids 1-32 and 75-89 (Figure 1b). This is exactly the same conformation adopted by $I27^{32\text{-}75}$ when unfolded

under force[7]. Hence, the extension after the mechanical unfolding of $I27^{2S\text{-}S}$ should be the same as for $I27^{32\text{-}75}$. Experimentally, we found that the mechanical unfolding of $I27^{2S\text{-}S}$ is characterized by an increment in contour length of ~11 nm (Figures S2, S6), the same value found for $I27^{32\text{-}75}$ in previous reports[8]. This result rules out the possibility that disulfides other than 24-55 and 32-75 are present in $I27^{2S\text{-}S}$ and assures that disulfide 32-75 is correctly established and buried in the fold of the protein, as explained below.

11 different disulfide configurations could be expected for $I27^{2S\text{-}S}$ depending on the total number of disulfides present in the protein and the residues involved in their formation (Table S2). In a previous work, we determined the end-to-end length of the transition state for the mechanical unfolding of I27 (13.4 amino acids)[1]. According to Equation S1, at F = 150 pN and considering a persistence length of 0.3 nm, x/L ~0.84. Therefore, the predicted increment in extension after the mechanical unfolding (Δx_u) of any I27 variant that contains disulfide bonds can be estimated according to the following expression:

$$\Delta x_u \text{ (nm)} = 0.84 \cdot [0.4 \cdot (n_{aa} - 13.4) + 0.8 \cdot n_{SS}] \qquad \text{(Equation S3)}$$

, where n_{aa} and n_{SS} are the number of amino acids and disulfides, respectively, subject to force after mechanical extension of the polypeptide. According to the results in Table S2, the ~11 nm experimental value for Δx_u is incompatible with any combination that includes disulfides other than 24-55 or 32-75. In addition, the experimental Δx_u agrees with the presence of disulfide 32-75, as any configuration not containing this disulfide would be characterized by different Δx_u values. Therefore, this result shows that disulfide 32-75 is buried in the fold of $I27^{2S\text{-}S}$ and cannot be reduced unless the protein is mechanically unfolded.

Preferential cleavage of disulfide 32-75 over 24-55 by L-Cys.

The pathways arising from the initial reduction of disulfide 32-75 are described in Figure 2. Figure S4 shows the alternative pathways if disulfide 24-55 was reduced first. In that case, three different combinations of step sizes would be expected. As disulfide 24-55 is off the force pathway after unfolding of $I27^{2S\text{-}S}$ (Figure 1b), its cleavage does not translate into an extension of the polypeptide. However, the reductions occurring afterwards are characterized by specific step sizes (Figure S4). In the event that disulfide 32-75 is cleaved by an external L-Cys molecule, a ~14-nm step would be expected, whereas the intramolecular attack by Cys55 would generate two combinations of step sizes (8+6, or 7+7). Figure 1e shows that the ~14-nm steps are extremely rare events, suggesting that disulfide 24-55 is present in the majority of $I27^{2S\text{-}S}$ modules and that is hardly ever cleaved before disulfide 32-75. Regarding the size of the alternative steps developing from the initial reduction of disulfide 24-55 (6, 7, and 8 nm), they overlap with some of the steps originating from the initial reduction of disulfide 32-75 (Figure 2). However, in the latter case, they are always accompanied by a 4-nm step, which is absent in the former set of pathways. Taking this information into account, we could assign most of the experimental traces unambiguously. We estimate that disulfide 32-75 is cleaved first in ~95% of the events. Our observation is in agreement with the fact that disulfide

32-75 is more reactive than disulfide 24-55 in the single-disulfide I27 variants[9] and the increased reactivity of L-Cys towards a force-bearing disulfide[10].

Kinetic model.

In the kinetic model in Figure 3a, the initial reduction of disulfide 32-75 occurs by the nucleophilic attack of an external L-Cys molecule on either Cys75 or Cys32. Both pathways are first-order reactions characterized by rate constants k_1 and k_7 that extend the polypeptide by 4 nm. The fate of disulfide 24-55 depends on the pathway followed to cleave disulfide 32-75. If L-Cys attacks on position 75, according to Equations 1 and 2, a reactive Cys is generated in the proximity of disulfide 24-55 (Figure 3a, top). Hence, from this branching point disulfide 24-55 can be cleaved following three competing reaction pathways. The intermolecular rupture of disulfide 24-55 by an external L-Cys extends the polypeptide by 10 nm to the fully reduced and extended protein (Figures 1d, 2a), and is characterized by a first-order rate constant, k_4. This intermolecular reaction competes with the intramolecular attack by Cys32 on either Cys55 or Cys24, which render steps of 3 nm and 8 nm, respectively (Figures 2b, c). In our model, we consider that these intramolecular reactions show zero-order kinetics with constants k_2 and k_5, respectively, and that they are followed by the attack of a new L-Cys molecule to render the fully reduced protein. The three competing pathways do not occur if the original cleavage of disulfide 32-75 happens through nucleophilic attack on Cys32 (Figure 3a, bottom). In this case, Cys32 forms a mixed disulfide with the L-Cys molecule and remains inactive, and only the first-order nucleophilic attack by a new L-Cys can cleave disulfide 24-55 to completely extend the protein.

For the 3- and 8-nm steps, there is a straightforward relationship linking their frequency of appearance to the value of the rate constants:

$$f(3) = \frac{k_1}{k_1 + k_7} \cdot \frac{k_2}{k_2 + k_5 + k_4 \cdot [L-Cys]} \quad \text{(Equation S4)}$$

$$f(8) = \frac{k_1}{k_1 + k_7} \cdot \frac{k_5}{k_2 + k_5 + k_4 \cdot [L-Cys]} \quad \text{(Equation S5)}$$

Equations S4 and S5 take into account the joint probability that disulfide 32-75 is attacked on position 75 and disulfide 24-55 is attacked on the corresponding sulfur atom (Figure 3a, top). Similarly, the following equation can be derived for the frequency of appearance of the 10-nm events:

$$f(10) = 1 - f(3) - f(8)$$

$$f(10) = 1 - \frac{k_1}{k_1 + k_7} \cdot \frac{k_a}{k_a + \cdot [L-Cys]} \quad \text{(Equation S6)}$$

where $k_a = \frac{k_2 + k_5}{k_4}$.

Force dependency of rate constants.

The reaction rates of simple thiol/disulfide exchange reactions have been shown to increase exponentially with force according to the Bell model[8,10,11]:

$$k(F) = k(F=0) \cdot e^{\frac{F \cdot \Delta x}{K_B \cdot T}} \quad \text{(Equation S7)}$$

where $k(F=0)$ is the rate constant at zero force and Δx is the distance to the transition state of the reaction. In this work, we considered $\Delta x = 0.023$ nm[10].

The mixed disulfide between Cys32 and L-Cys is not resolved significantly in our experimental time scale.

In the kinetic model in Figure 3a, we considered that the cleavage of the mixed disulfide between L-Cys and Cys32 is slow and does not occur to a significant extent in our experimental conditions. This assumption implies that all the intramolecular thiol/disulfide exchange reactions arise from the original attack by an L-Cys molecule on position 75 (Figure 3a, top), which simplifies the interpretation of the experimental results. However, if the inert mixed disulfide was resolved by another L-Cys from the bathing solution, Cys32 may be rendered reactive (Figure S7a). The extent of this side reaction depends on the competition with the intermolecular cleavage of disulfide 24-55 governed by k_8. Three arguments can be put forward to support the assumption that the mixed disulfide is not significantly cleaved in our experiments, i.e. that $k_9 << k_8$. First, the mixed disulfide is not subject to force, while disulfide 24-55 is. Then, the cleavage of disulfide 24-55 at 250 pN is accelerated ~4 times with respect to zero force. In addition, from the two possibilities that exist to cleave the mixed disulfide, one of them occurs through an attack on Cys32. In this case, Cys32 would remain blocked. Only if the attack occurs on the L-Cys molecule can Cys32 be released (Figure S7a). Finally, unpublished data show that L-Cys inhibits the folding of $I27^{32-75}$ when forming a mixed disulfide with the unfolded polypeptide. Only if the folding time is long enough (> 20 seconds), can folding events be detected, reflecting the resolution of the mixed disulfide (data not shown). Thus, this suggests that the resolution of the mixed disulfides generally takes longer than the cleavage of disulfide 24-55 (Figure 3).

In order to get experimental evidence that the resolution of the mixed disulfide between L-Cys and Cys32 is not significant in our experimental conditions, we tested if the proportions of the different step sizes are force dependent. From the scheme in Figure S7a, it follows that if k_9 was the same order of magnitude as k_8, an increase in the force would differentially accelerate the rupture of disulfide 24-55. This would lead to an increase in the frequency of appearance of the 10-nm steps. We found that the frequencies of appearance of the 10-nm steps at 350 pN and 250 pN are coincident, even though k_8 is expected to increase ~1.8-2.0 times (Figures S7b, c). We also found that the ratio between the frequency of appearance of the 3- and 8-nm steps at 250 and 350 pN does not change, again supporting our kinetic model (Figure S7d). In addition, the rate constants obtained by the downhill simplex method from the data at 250 pN also

reproduce the experimental results at 350 pN (Figure S7e). All the previous results argue in favor of the approximation that k_9 is negligible in our experimental conditions.

Correction for the L-Cys concentration.

We found that insoluble aggregates slowly appeared over the course of the AFM experiments. Most probably, the aggregation reflects the oxidation of L-Cys to produce L-cystine, whose solubility in aqueous buffers is low[12]. Together with the binding of the free thiol of L-Cys to the gold surface, the oxidation of L-Cys may affect the effective concentration of L-Cys. We found that a plot of the rate of cleavage of disulfide 32-75 in $I27^{2S\text{-}S}$ *versus* L-Cys concentration did not intercept at the origin of coordinates (Figure S8), strongly suggesting that the effective L-Cys concentration is lower than expected. In order to correct for these effects, we employed previously reported values for the rate of reduction of $I27^{32\text{-}75}$ by L-Cys [10]. We considered a first-order rate constant at 250 pN of 75.6 $M^{-1}s^{-1}$ to calculate the actual L-Cys concentration from the experimental rates. Using this procedure, the concentrations of L-Cys are corrected by a factor that is approximately equal to the x-intercept in Figure S8b.

Determination of rate constants.

The transition rates between the states shown in Figure S9 (which is a simplified representation of the kinetic model in Figure 3a) were given by the L-cysteine concentration c as well as the force dependent parameters k_1 through k_8, yielding a system governed by the following coupled differential equations:

$$\frac{d[1]}{dt} = -ck_1[1] - ck_7[1] \qquad \text{(Equation S8)}$$

$$\frac{d[2]}{dt} = ck_1[1] - k_2[2] - ck_4[2] - k_5[2] \qquad \text{(Equation S9)}$$

$$\frac{d[3]}{dt} = k_2[2] - ck_3[3] \qquad \text{(Equation S10)}$$

$$\frac{d[4]}{dt} = k_5[2] - ck_6[4] \qquad \text{(Equation S11)}$$

$$\frac{d[5]}{dt} = ck_7[1] - ck_8[5] \qquad \text{(Equation S12)}$$

$$\frac{d[6]}{dt} = ck_3[3] + ck_4[2] + ck_6[4] + ck_8[5] \qquad \text{(Equation S13)}$$

We converted these equations into matrix form, and then used matrix algebra to find the eigenvalues and corresponding eigenvectors of the system's transition matrix. We could thus attain an analytical solution to the system, in the form of the probability of the system being in a certain state as a function of time. By initializing the system as being in state 1 (i.e. taking [1]=1 at t=0 as initial condition) we could compare the predicted outcome of the system z to the experimental data y for a given set of parameters (as seen in Figures 3e, S5).

We sought to find the optimal parameter values that best described the experimental data. For a given set of parameters (i.e. rate constants) the goodness of the fit was asserted by calculating the sum of the squared residuals at *N* uniformly spaced time points. This error sum was then computed for all four concentrations used in the experiments, and the total error sum was given as follows:

$$R = \sum_{i=1}^{4} \sum_{j=1}^{N} [y(c_i, t_j) - z(k_1 ... k_8, c_i, t_j)]^2 \qquad \text{(Equation S14)}$$

Seeking to minimize *R*, we used the downhill simplex method[7,13] to find the optimal parameter values $k_1 \ldots k_8$. However, before running the optimization, we could limit the parameter space by taking into account certain experimental measurements. These observations, detailed below, allowed us to determine or constrain some rate constants.

We used the end-point data in Figure 3b to estimate the relative value of k_1 and k_7. According to Equation S6, the extrapolated value of f(10) at [L-Cys] = 0 equals $\frac{k_7}{k_1 + k_7}$. Considering that the rate constant for the cleavage of disulfide 32-75 is 18.44 $M^{-1}s^{-1}$ (the same value used for correcting the concentration of L-Cys)[10], we calculated k_1 = 12.72 $M^{-1}s^{-1}$ and k_7 = 5.72 $M^{-1}s^{-1}$. In addition, taking into account all the experimental data at 250 pN, we observed that the frequency of appearance of the 3-nm steps is 3.8 times higher than that of the 8-nm step. Therefore, we introduced the constraint that $k_2/k_5 = 3.8$. We also considered that k_4 and k_8 are identical, as both represent the cleavage of disulfide 24-55 by an external L-Cys molecule.

Given all of these experimentally determined constraints we were left with two free parameters, which we took to be k_4 and k_5. The downhill simplex algorithm displayed robust convergence to the same parameter values for a wide variety of starting guesses. The values thus obtained are therefore likely to represent a global optimum. Interestingly, the relative reactivities of disulfides 32-75 and 24-55 within $I27^{2S\text{-}S}$, i.e. $\frac{k_4}{k_1 + k_7}$, matches the relative reactivity of the disulfides in the single-disulfide mutants $I27^{32\text{-}75}$ and $I27^{24\text{-}55}$ [9]. In this report, we did not investigate the values of k_3 and k_6.

Steered molecular dynamics simulations.
The structures in Figures 1, 4 and S3 were obtained from steered molecular dynamics simulations. The simulations were performed according to protocols described elsewhere[4,7].

SUPPLEMENTARY FIGURES

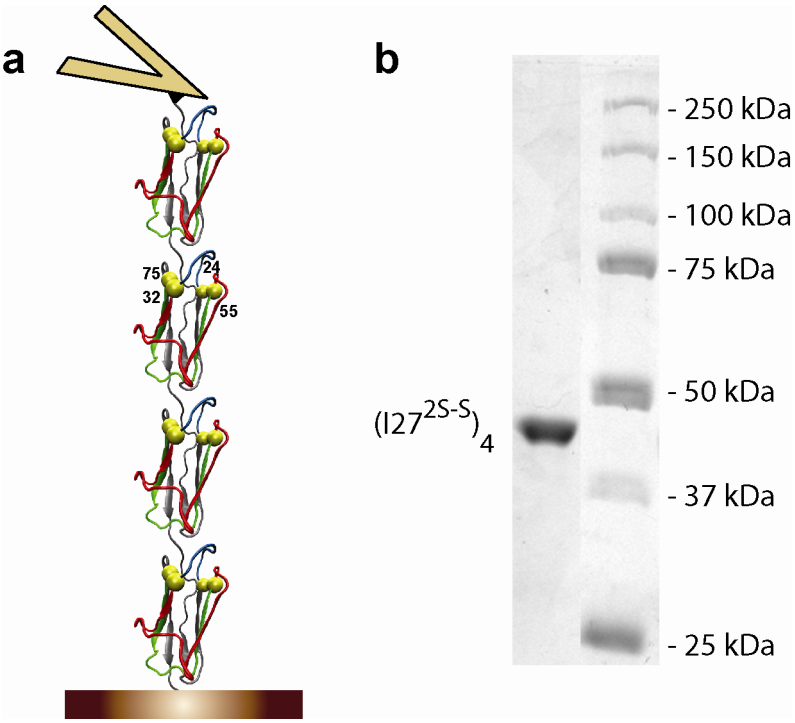

Figure S1. Experimental setup and production of $(I27^{2S-S})_4$. a, $(I27^{2S-S})_4$, a polyprotein based in the I27 protein that includes cysteine residues at position 24, 32, 55 and 75, is pulled with an atomic force microscope working in force-clamp mode. $(I27^{2S-S})_4$ forms disulfides between residues 24-55 and 32-75. **b,** $(I27^{2S-S})_4$ is purified to homogeneity. ~0.2 µg of purified protein were run in a 10% SDS-PAGE together with molecular weight markers (Precision Plus Protein Standards, Bio-Rad).

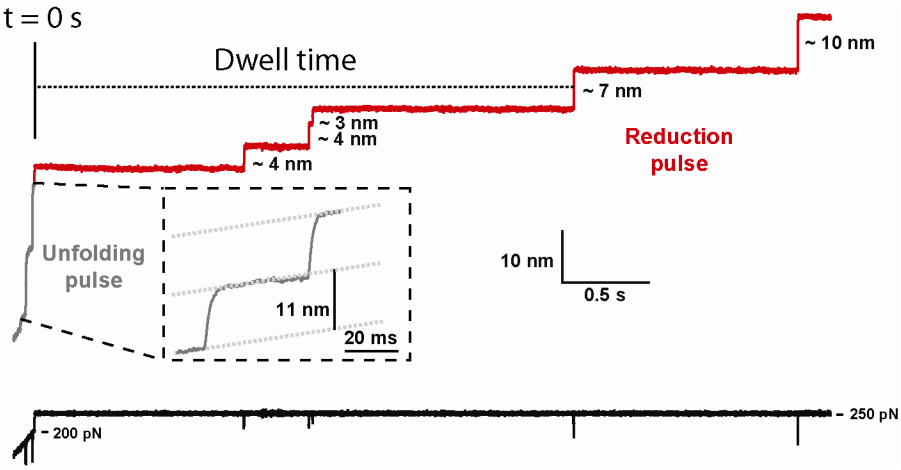

Figure S2. Experimental trace showing the unfolding and the reduction force pulses. We used a double pulse force protocol to study the unfolding of $(I27^{2S-S})_4$ and the subsequent reductions of its disulfides by the simple reducing agent L-Cys. In the first pulse, a 0.5-second linear ramp up to 200 pN was applied to the protein, which triggered the unfolding of the $I27^{2S-S}$ domains (in this particular trace, two domains unfolded). Then, the force was kept constant at 250 pN for 5-30 seconds to monitor the reduction events. An identical force protocol was used to measure reduction events for $(I27^{32-75})_8$ and $(I27^{24-55})_8$ (Figure 1). In order to calculate the dwell times of the reduction events, the beginning of the reduction pulse was considered as t = 0. The magnitude of the dwell time for the ~7-nm step is indicated.

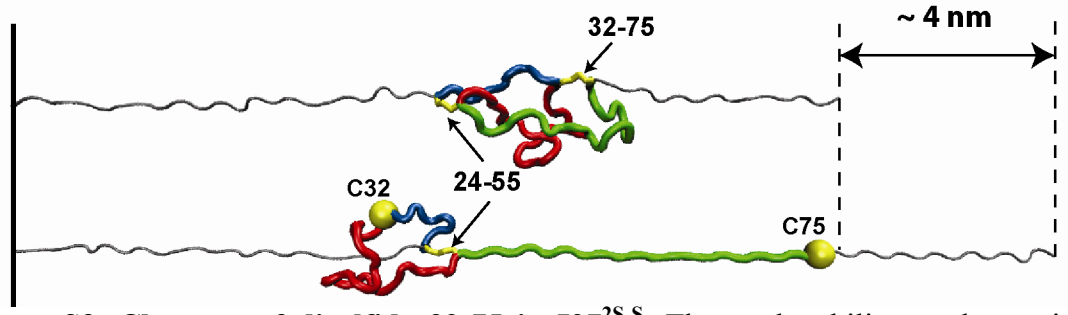

Figure S3. Cleavage of disulfide 32-75 in $I27^{2S\text{-}S}$. The nucleophilic attack on either Cys32 or Cys75 by an L-Cys molecule cleaves disulfide 32-75 and extends the polypeptide by 4 nm, corresponding to the release of 12 amino acids. After this reaction, Cys75 is pulled away from disulfide 24-55, while Cys32 remains proximal to this disulfide.

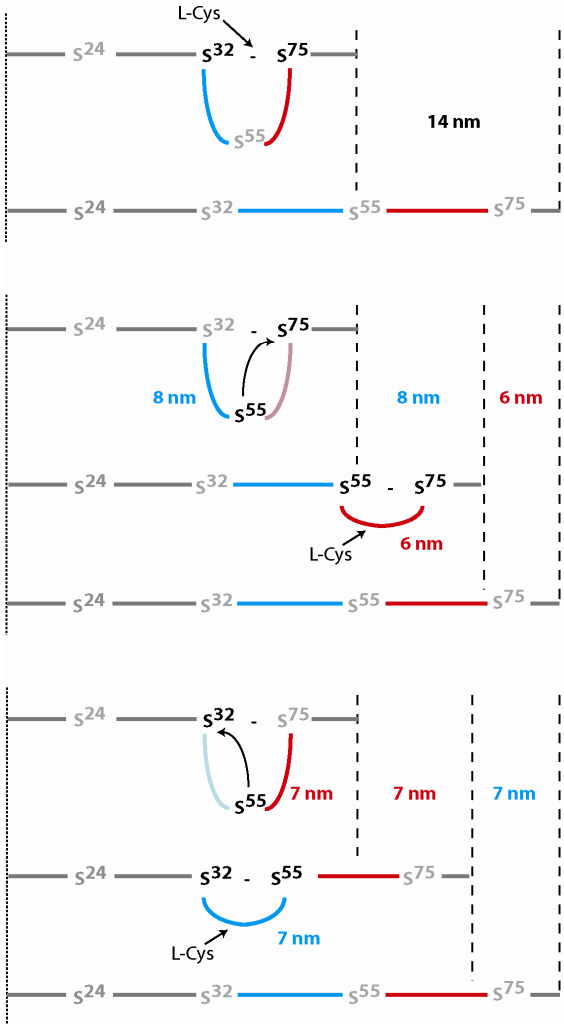

Figure S4. Pathways arising from the initial reduction of disulfide 24-55. Because disulfide 24-55 is not subject to force after the mechanical unfolding of $I27^{2S\text{-}S}$ (Figure 1b), the initial reduction of disulfide 24-55 does not generate a step under force-clamp conditions. The subsequent reduction of disulfide 32-75 can proceed through three different pathways. The cleavage by an external L-Cys molecule generates a ~14-nm step, whereas the intramolecular attacks by Cys55 produce two different combinations of step sizes, 8+6 and 7+7 nm.

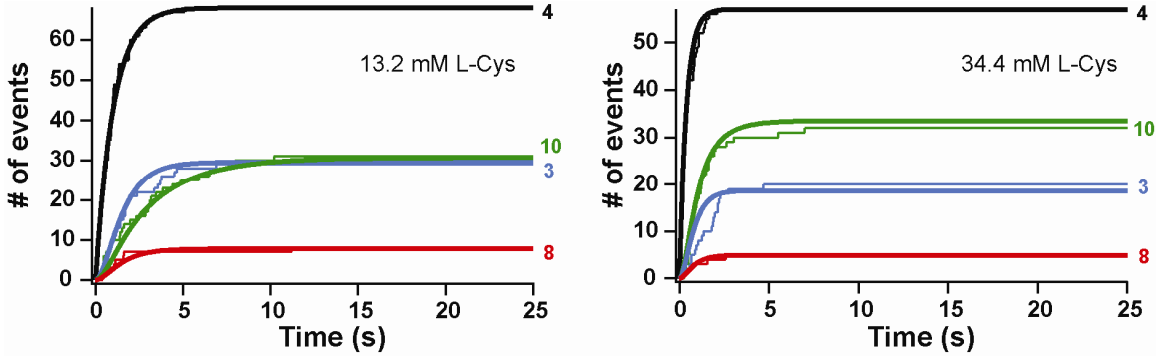

Figure S5. Kinetics of reduction of $I27^{2S\text{-}S}$ in the presence of 13.2 mM and 34.4 mM L-Cys. In order to prepare the figure, the same procedure described for Figure 3e in the main text was followed. (Thin lines) Time course of appearance of the different step sizes at 250 pN for two different concentrations of L-Cys. (Thick lines) Theoretical curves obtained from the rate constants determined using the downhill simplex method. Traces are identified by the magnitude of the experimentally measured steps.

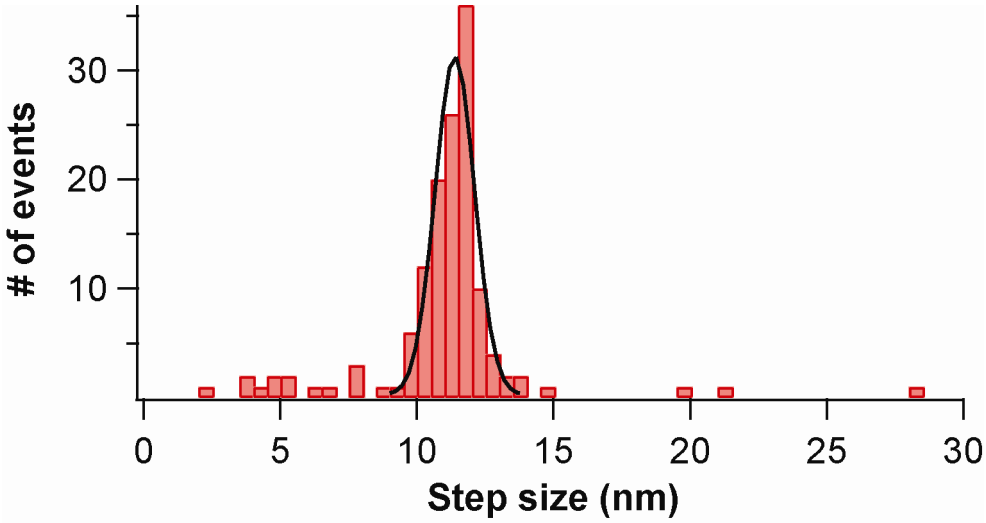

Figure S6. Distribution of step sizes measured during the unfolding of $(I27^{2S\text{-}S})_4$. This experiment was performed in the absence of reducing agents to avoid any interference coming from reduction reactions. The measured step size for the unfolding of the $I27^{2S\text{-}S}$ modules (Δx_u = 11 ± 1 nm) was calculated from a Gaussian fit to the histogram (n = 137).

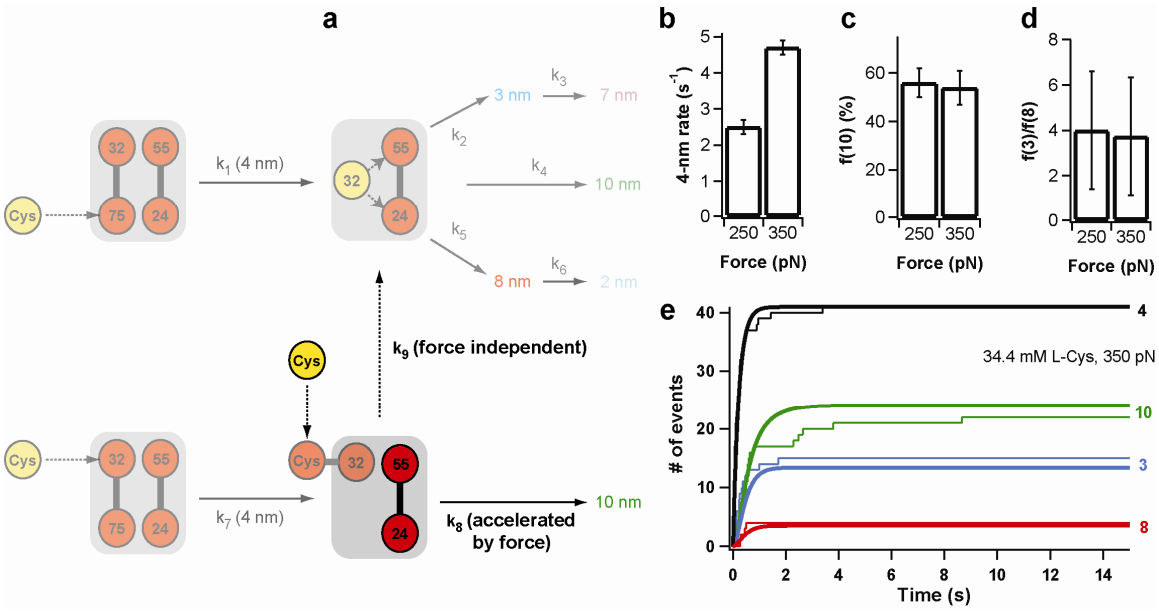

Figure S7. The resolution of the mixed disulfide involving Cys32 is negligible in our experimental conditions. a, Kinetic model that includes the cleavage by an external L-Cys molecule of the mixed disulfide intermediate involving Cys32. This attack would free Cys32 and enable the intramolecular thiol/disulfide exchanges, compromising our interpretation of the experimental results. The mixed disulfide between L-Cys and Cys32 is off the force pathway, whereas disulfide 24-55 is subject to force, implying that k_9 is expected to be force-independent while k_8 is accelerated by force[8,9]. k_8 and k_9 are the rates of two competing reaction pathways. Thus, if k_9 is not negligible, the frequency of appearance of the 10-nm step should increase with force, as the resolution of the mixed disulfide would become less prevalent. In order to test the prevalence of this side reaction, we reduced $I27^{2S\text{-}S}$ in the presence of 34.4 mM L-Cys at two different forces. **b,** Rate of appearance of the 4-nm steps, calculated from exponential fits to reconstructed traces. The error of the exponential fit is indicated. **c,** The frequency of appearance of the 10-nm steps does not increase with force, supporting the notion that k_9 is negligible. **d,** Ratio between the frequencies of appearance of the 3- and 8-nm steps. In c and d, error bars were estimated by bootstrapping. **e,** (Thin) Time course of appearance of the different step-sizes at 350 pN and 34.4 mM L-Cys. (Thick) Theoretical curves obtained from the rate constants determined using the downhill simplex method. Traces are identified by the magnitude of the experimentally measured steps.

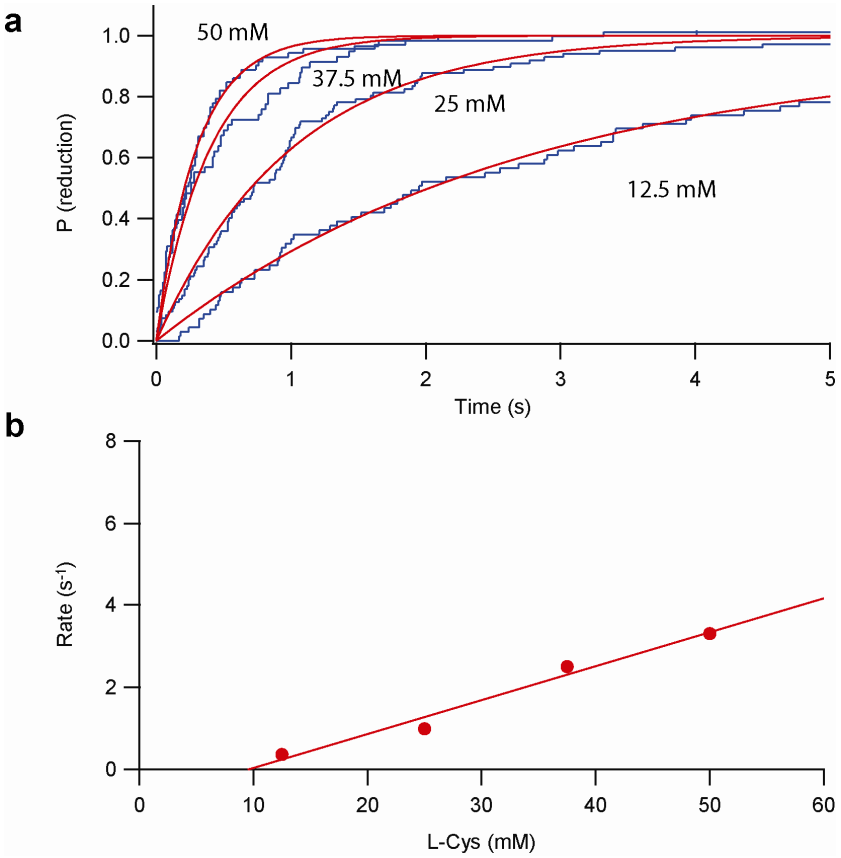

Figure S8. The effective concentration of L-Cys is lower than expected. a, The cumulative probability of reduction of disulfide 32-75 in $I27^{2S\text{-}S}$ is plotted for four different concentrations of L-Cys. Red lines are exponential fits used to calculate the rate of the reaction[8]. **b,** The plot showing the rate of reduction of disulfide 32-75 as calculated in (a) does not intercept at the origin of coordinates, showing that the effective concentration of L-Cys is lower than expected.

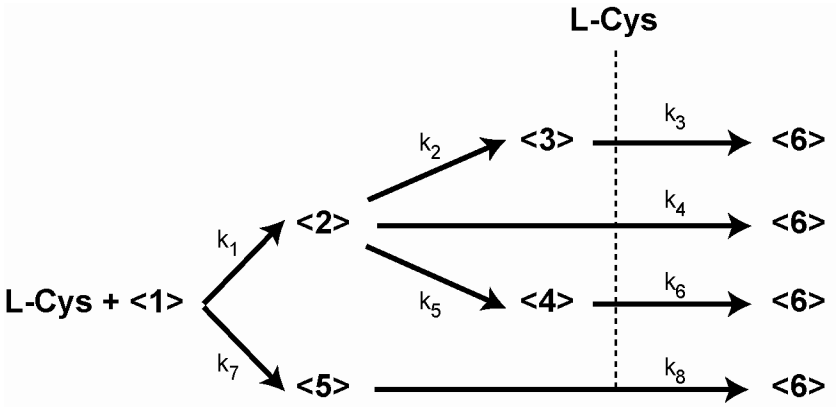

Figure S9. Simplified kinetic model. This simplified version of Figure 3a follows the nomenclature used in Equations S8-S13.

SUPPLEMENTARY TABLES

Cys24-Cys55	Cys32-Cys75
Glu-Ile-Cys24-Leu-Asp	Lys-His-Cys32-Gln-Trp
Gly-Lys-Cys55-His-Ile	Phe-Gln-Cys75-Ala-Asn

Table S1. Sequences surrounding the cysteine residues involved in the thiol/disulfide exchange reactions. Residues that are expected to be positively charged are marked in red.

Number of disulfides	Combination of disulfides	n_{aa}	n_{SS}	Predicted Δx_u, nm	Experimental Δx_u, nm
2	**24-55** **32-75**	44	1	11.0	
	24-75 **32-55**	36	1	8.3	
	24-32 **55-75**	58	2	16.3	
1	**24-32**	79	1	22.7	
	24-55	56	1	15.0	15.2 [9]
	24-75	36	1	8.3	
	32-55	64	1	17.8	
	32-75	44	1	11.0	11.0 [9]
	55-75	67	1	18.9	
0	-	89	0	25.4	24.5 [14]

Table S2. Predicted extensions after mechanical unfolding (Δx_u) for all the combinations of disulfides possible for $I27^{2S-S}$. n_{aa} and n_{SS} are the number of amino acids and disulfides, respectively, subject to force after mechanical extension of the polypeptide. Only the combinations marked in red are in agreement with the experimental value found for $I27^{2S-S}$ (Figures S2, S6).

SUPPLEMENTARY REFERENCES

1. Ainavarapu, S. R. et al. Contour length and refolding rate of a small protein controlled by engineered disulfide bonds. *Biophys J* **92**, 225-233 (2007).
2. Bustamante, C., Marko, J. F., Siggia, E. D. & Smith, S. Entropic elasticity of lambda-phage DNA. *Science* **265**, 1599-1600 (1994).
3. Carrion-Vazquez, M., Marszalek, P. E., Oberhauser, A. F. & Fernandez, J. M. Atomic force microscopy captures length phenotypes in single proteins. *Proc Natl Acad Sci U S A* **96**, 11288-11292 (1999).
4. Dougan, L. et al. Single homopolypeptide chains collapse into mechanically rigid conformations. *Proc Natl Acad Sci U S A* **106**, 12605-12610 (2009).
5. Grandbois, M. et al. How strong is a covalent bond? *Science* **283**, 1727-1730 (1999).
6. Alegre-Cebollada, J., Badilla, C. L. & Fernandez, J. M. Isopeptide bonds block the mechanical extension of pili in pathogenic Streptococcus pyogenes. *J Biol Chem* **285**, 11235-11242 (2010).
7. Wiita, A. P. et al. Probing the chemistry of thioredoxin catalysis with force. *Nature* **450**, 124-127 (2007).
8. Wiita, A. P., Ainavarapu, S. R., Huang, H. H. & Fernandez, J. M. Force-dependent chemical kinetics of disulfide bond reduction observed with single-molecule techniques. *Proc Natl Acad Sci U S A* **103**, 7222-7227 (2006).
9. Garcia-Manyes, S. et al. Force-activated reactivity switch in a bimolecular chemical reaction. *Nature Chemistry* **1**, 236-242 (2009).
10. Koti Ainavarapu, S. R. et al. Single-molecule force spectroscopy measurements of bond elongation during a bimolecular reaction. *J Am Chem Soc* **130**, 6479-6487 (2008).
11. Bell, G. I. Models for the specific adhesion of cells to cells. *Science* **200**, 618-627 (1978).
12. Apruzzese, F., Bottari, E. & Festa, M. R. Protonation equilibria and solubility of l-cystine. *Talanta* **56**, 459-469 (2002).
13. Press, W.H., Teukolsky, S.A., Vetterling, W.T. & Flannery, B.P., *Numerical Recipes in C - The Art of Scientific Computing*. (Cambridge University Press, Cambridge, UK, 1992).
14. Garcia-Manyes, S., Brujic, J., Badilla, C. L. & Fernandez, J. M. Force-clamp spectroscopy of single-protein monomers reveals the individual unfolding and folding pathways of I27 and ubiquitin. *Biophys J* **93**, 2436-2446 (2007).